Circular bubbles in a Hele-Shaw channel: a Hele-Shaw Newton's cradle

D. J. Booth, I. M. Griffiths and P. D. Howell

(Received xx; revised xx; accepted xx)

We consider the propagation of inviscid bubbles in a Hele-Shaw cell under a uniform background flow. We focus on the distinguished limit in which the hydrodynamic pressure gradient due to the external flow balances viscous drag effects due the thin liquid films between the bubbles and the cell walls (Bretherton 1961), with the ratio between these two effects measured by a single dimensionless parameter which we label δ. In this régime, we find that each bubble remains approximately circular, and its propagation velocity is determined by a net force balance. The analytical solution for the problem of an isolated bubble in an infinite Hele-Shaw cell is found to agree well with experimental data in the literature. In particular, we find that the bubble may move faster or slower than the background fluid speed, depending on whether $\delta > 1$ or $\delta < 1$, or precisely with the background flow if $\delta = 1$.

When the model is generalised to include the effects of multiple bubbles and boundaries in the Hele-Shaw cell, we still find that the sign of $\delta - 1$ causes striking changes in the qualitative behaviour. For a train of three or more bubbles moving along a Hele-Shaw channel, we observe longitudinal waves that propagate forwards or backwards along the bubble train, depending on whether $\delta > 1$ or $\delta < 1$, resembling a Hele-Shaw Newton's cradle.

1. Introduction

Many microfluidic experiments and devices involve generating bubbles and then transporting them along microfluidic channels (Huerre *et al.* 2014; Anna 2016; Gnyawali *et al.* 2017). The bubbles are often large enough (compared with the channel height) to be pancake-shaped, i.e. flattened against the top and bottom walls of the channel, but almost always small enough to remain approximately circular in plan view (see, e.g., Garstecki *et al.* 2004; Beatus *et al.* 2012; Shen *et al.* 2014; Gnyawali *et al.* 2017). In this paper we derive a simple model for the motion of approximately circular bubbles in a Hele-Shaw cell, then use it to describe bubble propagation along a microfluidic channel modelled as a long Hele-Shaw cell with side walls.

It was first shown by Taylor & Saffman (1959) that, in the limit of zero surface tension, a circular bubble in a Hele-Shaw channel travels at twice the speed of the outer liquid. More generally they found that, for a specified channel width, outer liquid speed and bubble area, one can achieve an arbitrary bubble speed; selecting a particular speed then specifies the bubble shape. Maruvada & Park (1996) generalised the Taylor–Saffman solution to describe an elliptical surfactant-laden bubble in a Hele-Shaw cell.

Complex analysis lends itself to Hele-Shaw flow problems since the pressure in the fluid is modelled by Laplace's equation. For example, Crowdy (2009) used complex variable methods to study co-travelling multiple bubbles in an infinite Hele-Shaw cell. As in the Taylor–Saffman problem, this model does not involve surface tension and suffers from the same degeneracy. The degeneracy was removed by Tanveer (1986), who used complex variable techniques to include surface tension in the Taylor–Saffman problem. In

particular, Tanveer showed that, in the limit of large surface tension, the bubble shape is circular. A class of exact solutions for an infinite stream of groups of bubbles was derived by Vasconcelos (1994) by adapting the method of Tanveer. While the papers referenced above concern the deformation of bubbles, with either weak or entirely absent surface tension, in this paper we focus on the régime where surface-tension effects dominate and the bubbles remain approximately circular, as is commonly seen in microfluidic experiments.

Bretherton (1961) studied an inviscid bubble moving through a viscous liquid in a tube in the limit of small capillary number Ca. Bretherton's analysis was modernised by Park & Homsy (1984) using matched asymptotic expansions, while applying the theory to two-phase flow in a Hele-Shaw cell. For our purposes, their main finding is that viscous flow in the thin liquid films between the bubble and the cell walls causes an additional pressure jump across the bubble–liquid interface, which is proportional to $\mathrm{Ca}^{2/3}$. This result was corroborated by Reinelt (1987), who further used numerical methods to extend the theory to $O(1)$ capillary numbers. Meiburg (1989) demonstrated numerically how Tanveer's solutions are modified by the inclusion of this additional pressure drop. The effective boundary condition used by Meiburg (1989) was improved by Burgess & Foster (1990), both to capture correctly the Bretherton pressure drop at the rear interface of a moving bubble, and to analyse inner regions where the liquid flow is approximately tangent to the bubble interface and the Park & Homsy (1984) model breaks down. Reichert *et al.* (2019) included the Bretherton pressure drop in their model for an isolated circular bubble in a Hele-Shaw cell with a uniform background flow. Reyssat (2014) also included the Bretherton drag force in his model for a bubble in a Hele-Shaw cell whose walls are slightly inclined to form a thin wedge, and observed that the bubble migrates out of the wedge to reduce its surface area.

Kopf-Sill & Homsy (1988) studied experimentally the velocities of variously shaped bubbles in a Hele-Shaw cell, in particular observing circular bubbles that always travelled more slowly than the background flow. However, Park *et al.* (1994) showed that this behaviour was due to the presence of surfactants, and their experiments showed circular bubbles moving more quickly than the background flow, though still less than twice as fast (the Taylor–Saffman limit). Similarly Reichert *et al.* (2019) found circular bubbles travelling faster than the outer liquid velocity but with a larger range of bubble velocities. Shen *et al.* (2014) investigated the motion of multiple droplets in a Hele-Shaw channel, observing behaviour including pair exchange, where a single droplet catches up to a pair of bubbles and then the leading bubble breaks away. Beatus *et al.* (2006, 2012) explored instabilities in a one-dimensional array of droplets, resulting in the formation of transverse and longitudinal waves. Their experimental observations were captured well by a model where the droplets are treated as dipoles, although in principle this approach is strictly valid only when the droplets are sufficiently well-separated.

Sarig *et al.* (2016) solved for the pressure field around two arbitrarily spaced and sized droplets in a Hele-Shaw cell, and performed a force balance to determine the bubble velocities, including an internal droplet friction as in Beatus *et al.* (2012). We adopt a similar methodology, except we use the boundary condition derived by Burgess & Foster (1990) instead of the empirical friction force. Sarig *et al.*'s results were further analysed by Green (2018), who showed that the dipole approximation of Beatus *et al.* (2012) works well even when the bubble spacing is rather small and extended the analysis to model an arbitrary number of bubbles in the large-spacing asymptotic limit.

In §2 we derive a model for a bubble being swept along by a uniform flow in a Hele-Shaw cell, in a distinguished asymptotic limit where the Bretherton pressure drop is of the same order as the Hele-Shaw viscous forces. In this régime, the bubble remains approximately

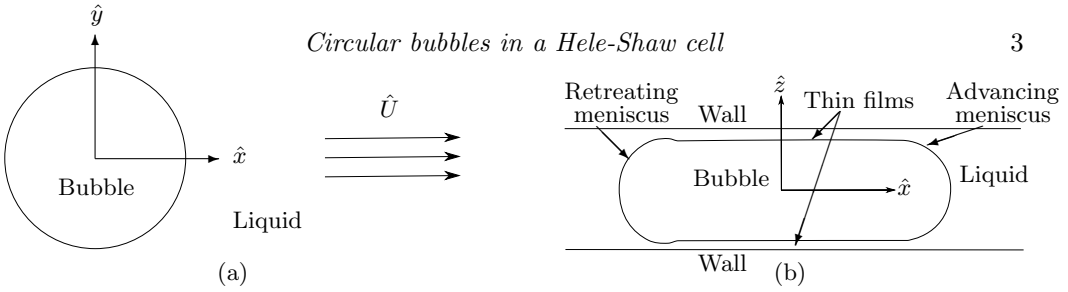

Figure 1: (a) Plan view of a bubble in a Hele-Shaw cell with a uniform background flow of speed $\hat{U}$. (b) Side view of the bubble.

circular, as in many microbubble experiments; the pressure in the surrounding liquid is found by solving a Neumann problem involving the *a priori* unknown bubble velocity, which is determined by a coupled net force balance on the bubble. We first derive the equation of motion for a single isolated bubble, which is equivalent to the model obtained by Reichert *et al.* (2019) using a dissipation argument. We then generalise the approach to describe an arbitrary collection of bubbles. In §3, we demonstrate possible analytical and numerical solution techniques by applying the model to some practically relevant examples. In particular, we show that proximity to cell boundaries and/or to other bubbles can either increase or decrease the bubble propagation speed, depending on the value of a single key dimensionless parameter. In a train of three or more bubbles, these effects result in the successive formation and breakup of bubble pairs in a phenomenon which resembles the dynamics in a Newton's cradle. We conclude in §4 by discussing our findings and the limitations of our model.

2. Model derivation

2.1. *Isolated bubble in an infinite medium*

We begin by considering an isolated bubble in a Hele-Shaw cell of thickness $\hat{h}$ parallel to the $(\hat{x},\hat{y})$-plane. Under the lubrication approximation, in the limit where $\hat{h}$ is much smaller than the horizontal dimensions of the cell and the bubble, the flow away from the bubble is governed by the Hele-Shaw equations:

$$\hat{\boldsymbol{v}} = \frac{3}{2}\hat{\boldsymbol{u}}\left(1 - \frac{4\hat{z}^2}{\hat{h}^2}\right), \tag{2.1a}$$

$$\hat{\boldsymbol{\nabla}} \cdot \hat{\boldsymbol{u}} = 0, \tag{2.1b}$$

$$\hat{\boldsymbol{u}} = -\frac{\hat{h}^2}{12\hat{\mu}}\hat{\boldsymbol{\nabla}}\hat{p}. \tag{2.1c}$$

Here, $\hat{\boldsymbol{v}}(\hat{x},\hat{y},\hat{z})$ is the full fluid velocity profile, $\hat{\boldsymbol{u}}(\hat{x},\hat{y})$ is the depth-averaged fluid velocity, $\hat{z} \in [-\hat{h}/2, \hat{h}/2]$ denotes the height coordinate, $\hat{p}(\hat{x},\hat{y})$ is the leading-order pressure, and $\hat{\mu}$ is the fluid viscosity.

In this section we focus on the simple model problem of a single bubble in a large cell with a prescribed uniform background flow of speed $\hat{U}$ in the $\hat{x}$-direction, which gives us the far-field condition

$$\hat{\boldsymbol{u}} \to \hat{U}\boldsymbol{i} \quad \text{as} \quad \hat{x}^2 + \hat{y}^2 \to \infty, \tag{2.2}$$

where $\boldsymbol{i}$ is the unit vector in the $\hat{x}$-direction.

Looking down on the cell from above (figure 1a), the boundary of the bubble appears to be a closed curve in the $(\hat{x},\hat{y})$-plane, on which we impose the effective boundary

conditions (Meiburg 1989)

$$\boldsymbol{n}\cdot\hat{\boldsymbol{u}} = \hat{U}_n, \tag{2.3a}$$

$$\hat{p}_b - \hat{p} = \frac{2\hat{\gamma}}{\hat{h}} + \frac{2\hat{\gamma}}{\hat{h}}\,\beta(\mathrm{Ca}_n)\mathrm{Ca}_n^{2/3} + \frac{\hat{\gamma}\pi}{4}\hat{\kappa}. \tag{2.3b}$$

Here, $\boldsymbol{n}$, $\hat{U}_n$ and $\hat{\kappa}$ are the outward-pointing normal, normal velocity and curvature of the apparent bubble boundary, respectively; $\hat{\gamma}$ is the surface-tension parameter, $\hat{p}_b$ is the uniform pressure inside the bubble, $\mathrm{Ca}_n = \hat{\mu}\hat{U}_n/\hat{\gamma}$ is the capillary number based on the normal velocity, and β is the Bretherton coefficient, whose value depends on whether the meniscus is advancing or retreating (Bretherton 1961; Halpern & Jensen 2002; Wong *et al.* 1995):

$$\beta(\mathrm{Ca}_n) = \begin{cases} \beta_1 \approx 3.88 & \text{when } \mathrm{Ca}_n > 0, \\ \beta_2 \approx -1.13 & \text{when } \mathrm{Ca}_n < 0. \end{cases} \tag{2.4}$$

The first term on the right-hand side of equation (2.3*b*) is the capillary pressure difference due to the meniscus at the bubble boundary, whose leading-order radius of curvature is given by $\hat{h}/2$. The second term containing the capillary number is the correction to the pressure difference in the limit $\mathrm{Ca}_n \ll 1$, derived in Bretherton's original paper (Bretherton 1961), due to the existence of the thin-film regions between the bubble and the walls of the cell (see figure 1b). The final term in (2.3*b*) captures the in-plane contribution to the curvature of the bubble interface, including the $\pi/4$ factor derived by Park & Homsy (1984).

We will further discuss the underlying assumptions and validity of the boundary condition (2.3*b*) below in §4.

2.2. *Non-dimensionalisation*

We non-dimensionalise the model (2.1)–(2.3), scaling lengths with a typical bubble radius, $\hat{R}$, and velocities with the far-field uniform flow speed, $\hat{U}$. We also scale $\hat{p}$ with $12\hat{\mu}\hat{U}R/\hat{h}^2$, $\hat{p}_b$ with $2\hat{\gamma}/\hat{h}$ and $\hat{\kappa}$ with $1/\hat{R}$. This process yields the following dimensionless system (in which dimensionless variables are denoted without hats):

$$\nabla^2 p = 0 \qquad \text{in} \quad \Omega, \tag{2.5a}$$

$$p_b - \frac{3\mathrm{Ca}}{\epsilon}p = 1 + \mathrm{Ca}^{2/3}\beta(U_n)U_n^{2/3} + \frac{\epsilon\pi}{4}\kappa \qquad \text{on} \quad \partial\Omega_b, \tag{2.5b}$$

$$\boldsymbol{n}\cdot\boldsymbol{\nabla}p = -U_n \qquad \text{on} \quad \partial\Omega_b, \tag{2.5c}$$

$$p \sim -x + o(1) \qquad \text{as} \quad x^2 + y^2 \to \infty, \tag{2.5d}$$

where Ω is the fluid domain and $\partial\Omega_b$ is the apparent bubble–fluid boundary in the (x, y)-plane, whose normal velocity is U_n. The far-field condition (2.5*d*) (with no logarithmic contribution) enforces conservation of the bubble area and thus in principle allows the bubble pressure p_b to be determined as part of the solution.

The system (2.5) contains two dimensionless parameters, the aspect ratio and the capillary number, defined by

$$\epsilon = \frac{\hat{h}}{2\hat{R}}, \qquad \mathrm{Ca} = \frac{\hat{\mu}\hat{U}}{\hat{\gamma}}, \tag{2.6}$$

respectively. For the boundary-value problem (2.5) to be valid, both of these parameters must be small: the Hele-Shaw model relies on ϵ being small, while the boundary condition (2.3*b*) is an asymptotic approximation in the limit $\mathrm{Ca} \to 0$ (Park & Homsy 1984). In the

boundary condition (2.5b), the dominant balance depends on the relative size of these two small parameters.

In this work, we study flows in which the Hele-Shaw pressure is of the same order as the Bretherton drag term, and equation (2.5b) shows that this occurs when $\mathrm{Ca} = O(\epsilon^3)$. Expanding p_b and κ as asymptotic expansions in powers of ϵ we then see that

$$p_{b_0} + \epsilon p_{b_1} + \epsilon^2 p_{b_2} - \underbrace{\frac{3\mathrm{Ca}}{\epsilon} p}_{O(\epsilon^2)} + O(\epsilon^3) \sim 1 + \frac{\epsilon\pi}{4}(\kappa_0 + \epsilon\kappa_1) + \underbrace{\beta \mathrm{Ca}^{2/3} U_n^{2/3}}_{O(\epsilon^2)} + O(\epsilon^3) \tag{2.7}$$

on $\partial\Omega_b$. At $O(1)$ we find that $p_{b_0} = 1$, indicating that the leading-order bubble pressure is determined by the capillary pressure jump across the meniscus. At $O(\epsilon)$ we obtain $\kappa_0 = 4p_{b_1}/\pi = \text{constant}$, which implies that the bubbles we are studying are circular to leading order in ϵ. By our choice of length-scale $\hat{R}$ we can take the bubble here to have unit dimensionless radius.

Since the bubble remains (approximately) circular for all time, the normal velocity on the boundary is just given by $U_n = \boldsymbol{U}_b \cdot \boldsymbol{n}$, where $\boldsymbol{U}_b = (U_b, V_b)$ is the constant bubble velocity. In terms of plane polar coordinates (r, θ) based on the bubble centre, we therefore find that the pressure in the liquid satisfies the problem

$$\nabla^2 p = 0 \qquad \text{in} \quad r > 1, \tag{2.8a}$$

$$\frac{\partial p}{\partial r} = -\boldsymbol{U}_b \cdot \boldsymbol{n} = -U_b \cos\theta - V_b \sin\theta \qquad \text{on} \quad r = 1, \tag{2.8b}$$

$$p \sim -r\cos\theta + o(1) \qquad \text{as} \quad r \to \infty. \tag{2.8c}$$

If $\boldsymbol{U}_b$ were known, then p would be uniquely determined by (2.8). To find the bubble velocity, we return to the boundary condition (2.7), which so far has been imposed up to $O(\epsilon)$. In principle the solvability condition at $O(\epsilon^2)$ determines $\boldsymbol{U}_b$ and closes the problem. As a shortcut to deriving this condition, we note that, for any smooth closed planar curve $\partial\Omega_b$ and with $\boldsymbol{k}$ denoting the unit vector in the z-direction,

$$\oint_{\partial\Omega_b} \boldsymbol{n}\,\mathrm{d}s = \oint_{\partial\Omega_b} \boldsymbol{k} \times \frac{\mathrm{d}\boldsymbol{r}}{\mathrm{d}s}\,\mathrm{d}s = \boldsymbol{0}, \qquad \oint_{\partial\Omega_b} \kappa\boldsymbol{n}\,\mathrm{d}s = \oint_{\partial\Omega_b} -\frac{\mathrm{d}^2\boldsymbol{r}}{\mathrm{d}s^2}\,\mathrm{d}s = \boldsymbol{0}, \tag{2.9}$$

by standard results from differential geometry (see, e.g., Kreyszig 1959, Chapter 2). We therefore obtain from (2.5b) the constraint

$$\oint_{\partial\Omega_b} -p\boldsymbol{n}\,\mathrm{d}s = \frac{\epsilon}{3\mathrm{Ca}^{1/3}} \oint_{\partial\Omega_b} \beta(\boldsymbol{U}_b \cdot \boldsymbol{n})(\boldsymbol{U}_b \cdot \boldsymbol{n})^{2/3}\boldsymbol{n}\,\mathrm{d}s, \tag{2.10}$$

which may be interpreted as a force balance on the bubble. To evaluate the integral on the right-hand side of (2.10), we now use the fact that, to leading order, the boundary $\partial\Omega_b$ is the unit circle, which we parameterise using

$$\boldsymbol{r}(s) = \frac{\boldsymbol{U}_b}{|\boldsymbol{U}_b|}\cos s + \frac{\boldsymbol{k} \times \boldsymbol{U}_b}{|\boldsymbol{U}_b|}\sin s. \tag{2.11a}$$

With β given by (2.4), we thus obtain

$$\begin{aligned}\oint_{\partial\Omega_b} \beta(\boldsymbol{U}_b \cdot \boldsymbol{n})(\boldsymbol{U}_b \cdot \boldsymbol{n})^{2/3}\boldsymbol{n}\,\mathrm{d}s &= \int_0^{2\pi} \frac{\beta(\cos s)|\cos s|^{2/3}}{|\boldsymbol{U}_b|^{1/3}} \left(\boldsymbol{U}_b \cos s + \boldsymbol{k} \times \boldsymbol{U}_b \sin s\right) \mathrm{d}s \\ &= (\beta_1 - \beta_2)\,\frac{\sqrt{\pi}\Gamma(4/3)}{\Gamma(11/6)}\,\frac{\boldsymbol{U}_b}{|\boldsymbol{U}_b|^{1/3}},\end{aligned} \tag{2.11b}$$

where Γ denotes the Gamma function. Thus (2.10) reduces to the following condition for

the bubble velocity:

$$\frac{\boldsymbol{U}_b}{|\boldsymbol{U}_b|^{1/3}} = \frac{\delta}{\pi} \oint_{r=1} -p\boldsymbol{n}\,\mathrm{d}s, \tag{2.12}$$

where we define the Bretherton parameter

$$\delta = \frac{3\sqrt{\pi}\Gamma(11/6)}{(\beta_1 - \beta_2)\Gamma(4/3)} \frac{\mathrm{Ca}^{1/3}}{\epsilon} \approx 1.12 \frac{\mathrm{Ca}^{1/3}}{\epsilon}. \tag{2.13}$$

By assumption, δ is $O(1)$ while ϵ and Ca are asymptotically small.

2.3. *Solution*

The problem (2.8) for an isolated circular bubble in an infinite cell is easily solved to obtain the pressure

$$p = \left(\frac{U_b - 1}{r} - r\right)\cos\theta + \frac{V_b}{r}\sin\theta. \tag{2.14}$$

We can thus evaluate the integral on the right-hand side of the force balance (2.12) to obtain an equation for the bubble velocity, namely

$$\frac{\boldsymbol{U}_b}{|\boldsymbol{U}_b|^{1/3}} = \delta(2\boldsymbol{i} - \boldsymbol{U}_b). \tag{2.15}$$

It follows that the bubble moves parallel to the background flow, as expected, with $\boldsymbol{U}_b = U_b\boldsymbol{i}$, where U_b satisfies the algebraic equation

$$\frac{U_b^{2/3}}{2 - U_b} = \delta. \tag{2.16}$$

The equation (2.16) for the bubble speed is equivalent to that found in Reichert *et al.* (2019), using a laborious viscous dissipation argument. (In Reichert *et al.* (2019) the constant of proportionality in (2.13) is found to be 1.20 rather than 1.12, due to inaccurate calculation of the integral and the Bretherton constants. Their method involves solution for the height of the thin liquid films above and below the bubble, followed by calculation of the viscous dissipation due to the thin films.) We note that equation (2.16) may be transformed into a cubic and thus solved explicitly for U_b; however the resulting expression is unwieldy and not particularly illuminating.

We plot the prediction (2.16) for the bubble velocity U_b versus the Bretherton parameter δ in figure 2, which shows good agreement with experimental data taken from Reichert *et al.* (2019); Park *et al.* (1994). We observe that U_b is an increasing function of δ; from (2.13) we see that δ is proportional to the bubble radius $\hat{R}$, which implies that larger bubbles should travel faster. As $\delta \to 0$, the Bretherton drag term dominates and $U_b \sim (2\delta)^{3/2}$. At the other extreme where $\delta \gg 1$, we recover the traditional Taylor–Saffman result (Taylor & Saffman 1959) of the bubble moving twice as fast as the outer flow. However, we note that the assumption of the bubble remaining approximately circular eventually fails if δ is too large. From (2.7) we observe that variations in the bubble curvature are of order $\delta^2\epsilon$, which is assumed to be small. We conclude that our model remains valid when δ is large, provided $1 \ll \delta \ll \epsilon^{-1/2}$.

From equation (2.16) we observe a transition in behaviour at $\delta = 1$: if $\delta < 1$ the bubble moves slower than the outer flow ($U_b < 1$) while if $\delta > 1$ the bubble moves faster than the outer flow ($U_b > 1$). The critical case where $U_b = 1$, so the bubble moves with the external flow, corresponds to the particular solution of the problem where $p \equiv -x$. We see that this solution satisfies (2.8) provided $(U_b, V_b) = (1, 0)$, and the force balance (2.12) is also satisfied provided $\delta = 1$.

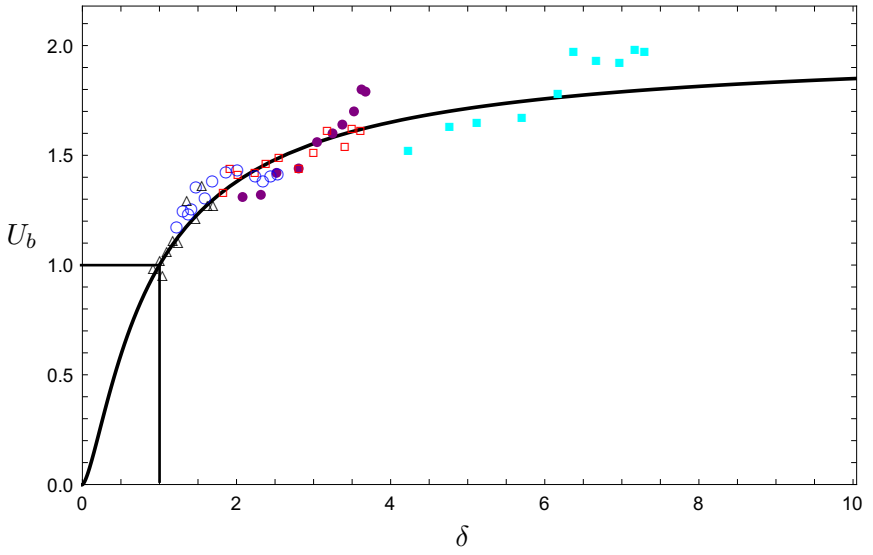

Figure 2: The ratio U_b of the bubble velocity to the outer fluid velocity as a function of the Bretherton parameter, δ. The solid curve shows the model prediction (2.16). The points show experimental data: ■ ($\epsilon = 0.035$) and ● ($\epsilon = 0.071$) from Park *et al.* (1994), with Ca in the range 2.3–12.7 $\times\, 10^{-3}$; □ ($\epsilon = 0.044$), ○ ($\epsilon = 0.07$), and △ ($\epsilon = 0.091$) from Reichert *et al.* (2019), with Ca in the range 0.4–6.0 $\times\, 10^{-3}$.

2.4. *The N-bubble problem*

It is straightforward to generalise the model derived above to describe a system of N bubbles. For the moment we continue to treat the Hele-Shaw cell containing the bubbles as effectively infinite, with a uniform flow imposed at infinity; the effects of cell boundaries will be incorporated below.

As in §2.2, each bubble remains circular (to leading order), with dimensionless radius R_k and velocity $\boldsymbol{U}_k$, say, for $1 \leqslant k \leqslant N$. The dimensionless pressure in the liquid domain Ω therefore satisfies

$$\nabla^2 p = 0 \qquad \text{in} \quad \Omega, \tag{2.17a}$$

$$\boldsymbol{n} \cdot \boldsymbol{\nabla} p = -\boldsymbol{U}_k \cdot \boldsymbol{n} \qquad \text{on} \quad \partial\Omega_k, \tag{2.17b}$$

$$\boldsymbol{\nabla} p \to -\boldsymbol{i} \qquad \text{as} \quad x^2 + y^2 \to \infty, \tag{2.17c}$$

where $\partial\Omega_k$ denotes the (circular) boundary of the k^{th} bubble. In principle, p would thus be determined if we knew the velocity $\boldsymbol{U}_k$ of each bubble. Indeed, the boundary-value problem described in (2.17) would then be equivalent to finding the velocity potential exterior to a collection of moving bodies or stirrers in two-dimensional irrotational flow with no circulation. The two-body version of this problem has been solved by Tchieu *et al.* (2010), and general integral expressions for the velocity potential due to any finite number of moving bodies are given by Crowdy (2008).

In the present problem, however, the bubble velocities are not known in advance. As in §2.2, the required equation of motion is obtained by performing an effective force balance, which here leads to

$$\frac{\boldsymbol{U}_k}{|\boldsymbol{U}_k|^{1/3}} = \frac{\delta}{\pi R_k} \oint_{\partial\Omega_k} -p\boldsymbol{n}\, \mathrm{d}s. \tag{2.18}$$

Again we notice that $p = -x$ is a solution to the problem (2.17) if and only if all of

the bubbles move at the same velocity $\boldsymbol{U}_k = \boldsymbol{i}$ for all k. The force balance (2.18) then requires $\delta R_k = 1$. Therefore it is possible for all of the bubbles to be convected at the same velocity as the outer flow, regardless of their position, only when all the bubbles are the same size.

Thus far we have formulated a general model for the motion of approximately circular bubbles in a Hele-Shaw cell and solved the model explicitly for the simplest possible case of a single isolated bubble. In the next section we use the model to analyse some more complicated examples, which illustrate the effects of walls on the bubble motion and the interactions between multiple bubbles.

3. Examples

3.1. *Isolated bubble near a wall*

Next we consider the case of a single bubble in a semi-infinite Hele-Shaw cell ($y > 0$) with an impermeable wall at $y = 0$ and a uniform flow $-\boldsymbol{\nabla} p \sim \boldsymbol{i}$ at infinity. The bubble is taken to have unit dimensionless radius with its centre a dimensionless distance $a > 1$ away from the boundary. The following analysis allows us to examine how proximity to a wall affects the velocity of the bubble, and also illustrates the application of complex variable methods to our model. This formulation is equivalent to the problem of two identical bubbles in an infinite cell with their centres separated by $2a$ and lined up perpendicular to the outer flow direction, with the wall representing the line of symmetry between them. The corresponding two-bubble problem was solved by Sarig *et al.* (2016) using bipolar coordinates rather than complex variables. We choose the bubble centre to be instantaneously at $z = x + \mathrm{i}y = a\mathrm{i}$, so that the domain of interest is $\Omega = \{z : \mathrm{Im}(z) > 0, |z - a\mathrm{i}| > 1\}$.

Since p satisfies Laplace's equation, we introduce a complex potential $w(z) = -p + \mathrm{i}\psi$, where ψ is the streamfunction. The problem is then to find a holomorphic function $w(z)$ in the region Ω such that

$$\mathrm{Im}[w(z)] = 0 \qquad \text{on} \quad \mathrm{Im}(z) = 0, \tag{3.1a}$$

$$\mathrm{Im}[w(z)] = q + \mathrm{Im}\left[\overline{\mathcal{U}}_b z\right] \qquad \text{on} \quad |z - a\mathrm{i}| = 1, \tag{3.1b}$$

$$w(z) \sim z \qquad \text{as} \quad z \to \infty. \tag{3.1c}$$

Both the complex bubble velocity $\mathcal{U}_b = U_b + \mathrm{i}V_b$ and the real constant q are *a priori* unknown; q represents the flux of liquid through the gap between the bubble and the wall (relative to the moving bubble). Once we have solved for w, the equation of motion (2.12) may be imposed by evaluating

$$\frac{1}{\mathrm{i}\pi}\oint_{\partial\Omega_b} w(z)\,\mathrm{d}z = -\mathcal{U}_b + \frac{1}{\pi}\oint_{\partial\Omega_b} p\mathrm{i}\,\mathrm{d}z = -\mathcal{U}_b + \frac{\mathcal{U}_b}{\delta\,|\mathcal{U}_b|^{1/3}}. \tag{3.2}$$

We proceed by conformally mapping Ω onto a concentric annulus, where the problem becomes solvable with standard techniques. Following the mapping

$$\zeta = f(z) = \frac{z - \mathrm{i}\sqrt{a^2 - 1}}{z + \mathrm{i}\sqrt{a^2 - 1}}, \tag{3.3}$$

the solution domain in the ζ-plane is $A = \{\zeta : X < |\zeta| < 1\}$, where

$$X = a - \sqrt{a^2 - 1}. \tag{3.4}$$

Writing the complex potential in the form $w(z) = z + W\big(f(z)\big)$, we find that W is

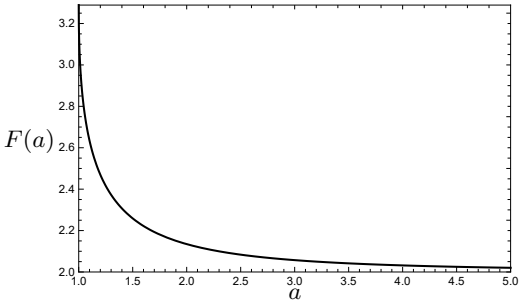

Figure 3: The function $F(a)$ defined by (3.10).

holomorphic on A and satisfies the boundary conditions

$$\mathrm{Im}[W(\zeta)] = 0 \qquad \text{on} \quad |\zeta| = 1, \tag{3.5a}$$

$$\mathrm{Im}[W(\zeta)] = q - \mathrm{Im}\left[\alpha\left(\frac{1+\zeta}{1-\zeta}\right)\right] \qquad \text{on} \quad |\zeta| = X, \tag{3.5b}$$

where $\alpha = \left(1 - \overline{\mathcal{U}}_b\right) \mathrm{i}\sqrt{a^2-1}$.

We then find that the *a priori* unknown flux q is given by

$$q = \mathrm{Im}(\alpha) = (1 - U_b)\sqrt{a^2-1}, \tag{3.6}$$

and the complex potential in the ζ-plane is given by

$$W(\zeta) = \sum_{n=1}^{\infty} \frac{2X^{2n}}{1 - X^{2n}}(\alpha\zeta^n + \overline{\alpha}\zeta^{-n}). \tag{3.7}$$

We can thus calculate the integral on the left-hand side of equation (3.2) by transforming into the ζ-plane and then using Cauchy's Residue Theorem to obtain

$$\frac{1}{\mathrm{i}\pi}\oint_{\partial\Omega_b} w(z)\,\mathrm{d}z = \frac{2\sqrt{a^2-1}}{\pi}\oint_{|\zeta|=X} \frac{W(\zeta)}{(\zeta-1)^2}\,\mathrm{d}\zeta = (1 - \mathcal{U}_b)F(a), \tag{3.8}$$

where

$$F(a) = 8\left(a^2 - 1\right)\sum_{n=1}^{\infty} \frac{nX^{2n}}{1 - X^{2n}}, \tag{3.9}$$

with X given as a function of a by (3.4). The formula (3.9) may be written in closed form as

$$F(a) = 2(a^2 - 1)\frac{\Psi'_{X^2}(1)}{\log^2 X}, \tag{3.10}$$

in which Ψ_{X^2} denotes the q-digamma function (Salem 2012), defined by

$$\Psi_q(z) = \frac{1}{\Gamma_q(z)}\frac{\mathrm{d}\Gamma_q(z)}{\mathrm{d}z}, \tag{3.11}$$

where Γ_q is the q-gamma function (Askey 1978). As shown in figure 3, $F(a)$ is a decreasing function of a, with $F(1) = \pi^2/3$ and $F(a) \to 2$ as $a \to \infty$.

Comparing imaginary parts in equation (3.2) we find that $V_b = 0$, so the bubble moves parallel to the wall. Then equating real parts in equation (3.2), the bubble's velocity in

the x-direction is found to satisfy the algebraic equation

$$\frac{U_b^{2/3}}{(1-U_b)F(a)+U_b} = \delta. \tag{3.12}$$

Once again (3.12) gives us a cubic that in principle can be solved explicitly for the dimensionless bubble velocity U_b. Rather than writing this complicated expression out explicitly, below we briefly examine the possible limiting cases.

First we observe that $U_b = 1$ when $\delta = 1$, so the bubble moves precisely with the external flow at this same critical value of the Bretherton parameter, regardless of the distance from the wall. As noted in §2.3, this special case corresponds to the particular solution where $p = -x$. For the extreme values of the Bretherton parameter δ, using (3.12) we derive the limits

$$U_b \to \frac{F(a)}{F(a)-1} \qquad \text{as} \quad \delta \to \infty, \tag{3.13a}$$

$$U_b \sim (\delta F(a))^{3/2} \qquad \text{as} \quad \delta \to 0. \tag{3.13b}$$

Taking the derivative of (3.12) with respect to δ we find

$$\frac{\partial U_b}{\partial \delta} = \frac{3U_b}{\delta\left[3\delta\big(F(a)-1\big)U_b^{1/3}+2\right]} > 0, \tag{3.14}$$

so U_b is a strictly increasing function of δ. It follows that $U_b > 1$ when $\delta > 1$ and *vice versa*.

As noted above, $F(a) \to 2$ as $a \to \infty$, so in this limit (3.12) reduces to the result (2.16) for a bubble in an infinite fluid medium, as expected. Similarly we can look at the limit $a \to 1$ in which the bubble touches the wall. Since $F(1) = \pi^2/3$, the bubble velocity tends to a non-zero value, which depends on the Bretherton parameter through the relation

$$\frac{3U_b^{2/3}}{\pi^2-(\pi^2-3)U_b} = \delta. \tag{3.15}$$

For intermediate values of a, we find that

$$\frac{\partial U_b}{\partial a} = \left[\frac{-\delta F'(a)}{\delta(F(a)-1)+\frac{2}{3}U_b^{-1/3}}\right](U_b-1), \tag{3.16}$$

in which the term in square brackets is positive. It follows that U_b is a decreasing function of a when $\delta < 1$, but an increasing function of a when $\delta > 1$.

The behaviour of the bubble velocity as the parameters a and δ are varied is shown in figure 4. As predicted, we observe that the presence of the wall either increases or decreases the bubble velocity, depending on whether $\delta < 1$ or $\delta > 1$, respectively. At the critical value of $\delta = 1$ we have $U_b = 1$ and the distance from the wall no longer matters.

At first glance it appears paradoxical that proximity to the wall may cause the bubble either to speed up or slow down, depending on the size of δ, but the behaviour may be explained as follows. By using the boundary condition (2.17b) and integration by parts, the force balance (2.18) may be rewritten as

$$\boldsymbol{U}_b\left(1+\frac{1}{\delta|\boldsymbol{U}_b|^{1/3}}\right) = \frac{1}{\pi}\oint_{\partial\Omega_b}\boldsymbol{u}\,\mathrm{d}s, \tag{3.17}$$

where $\boldsymbol{u} = (u,v)^{\mathrm{T}} = -\boldsymbol{\nabla}p$ is the dimensionless liquid velocity. For an isolated bubble,

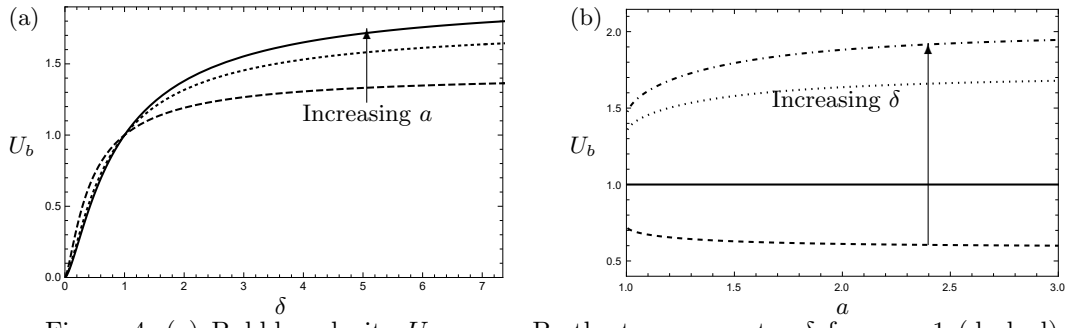

Figure 4: (a) Bubble velocity U_b versus Bretherton parameter δ for $a = 1$ (dashed), 1.5 (dotted) and ∞ (solid). (b) Bubble velocity U_b versus distance a from the wall for Bretherton parameter $\delta = 1/2$ (dotted), 1 (solid), 5 (dashed), $\delta = \infty$ (dot-dashed).

with the pressure given by (2.14), the integral on the right-hand side of (3.17) is easily calculated to be $2\boldsymbol{i}$, reproducing the equation of motion (2.15), and in general this term captures the influence of the outer flow on the bubble motion.

Now, what happens when a wall is introduced next to the moving bubble? From (3.6), we can calculate the average flow speed through the gap between the bubble and the wall (relative to the moving bubble) as

$$\frac{1}{a-1}\int_0^{a-1}(u-U_b)\,\mathrm{d}y = \frac{q}{a-1} = (1-U_b)\sqrt{\frac{a+1}{a-1}}. \tag{3.18}$$

First suppose the bubble is moving more slowly than the external flow, so $U_b < 1$. The right-hand side of equation (3.18) increases as the separation $a-1$ between the bubble and the wall decreases, measuring the acceleration of the liquid as it squeezes between the bubble and the wall. We find that the average velocity on the bubble surface thus increases and, according to (3.17), the bubble velocity also increases (relative to an isolated bubble). The horizontal component of the right-hand side of (3.17) may be calculated as

$$\frac{1}{\pi}\oint_{\partial\Omega_b} u\,\mathrm{d}s = 2 + (1-U_b)\big(F(a)-2\big), \tag{3.19}$$

which indeed increases as a decreases when $U_b < 1$.

On the other hand, if the bubble moves more quickly than the external flow ($U_b > 1$), then the liquid is squeezed backwards through the gap between the bubble and the wall so, by the same argument, the integral on the right-hand side of (3.17) and the bubble velocity should both decrease. This physical reasoning indeed agrees with the behaviour observed in figure 4. As noted above, the bubble travels faster or slower than the external flow depending on whether $\delta < 1$ or $\delta > 1$, and the effect of proximity to the wall is accordingly either to speed up or to slow down the bubble.

3.2. *Isolated bubble in a channel*

Next we consider the motion of a singular bubble of unit radius in a Hele-Shaw channel of width $W > 2$, between impermeable walls at $y = \pm W/2$. We again impose a uniform flow with $p \sim -x$ at infinity and, without loss of generality, take the bubble centre to be instantaneously at $(x, y) = (0, y_b)$, where $|y_b| < W/2 - 1$. It may then be shown that p is an odd function of x, and it follows from (2.12) that $V_b = 0$. Thus a single bubble in a channel will continue moving parallel to the outer flow no matter where in the channel it is initially placed.

To facilitate numerical solution, we pose the problem in terms of the streamfunction ψ,

which satisfies Dirichlet boundary conditions:

$$\psi(x,y) = \pm\frac{W}{2} \qquad \text{at} \quad y = \pm\frac{W}{2}, \tag{3.20a}$$

$$\psi(x,y) = q + U_b y \qquad \text{at} \quad x^2 + (y-y_b)^2 = 1, \tag{3.20b}$$

$$\psi(x,y) \to y \qquad \text{as} \quad x \to \pm\infty. \tag{3.20c}$$

The *a priori* unknown constant q is in principle determined by the constraint

$$\oint_{\partial\Omega_b} \frac{\partial\psi}{\partial n}\,\mathrm{d}s = 0, \tag{3.21}$$

which follows from single-valuedness of the pressure. The streamfunction is then decomposed as $\psi = U_b y + (1-U_b)\psi_1 + q\psi_2$, where each ψ_k satisfies a normalised boundary-value problem that is independent of q and U_b. We solve for ψ_1 and ψ_2 using finite element methods and then compute the four integrals

$$I_k = \frac{1}{\pi}\oint_{\partial\Omega_b}\left(\frac{\partial\psi_k}{\partial x}\,\mathrm{d}y - \frac{\partial\psi_k}{\partial y}\,\mathrm{d}x\right), \tag{3.22a}$$

$$J_k = \frac{1}{\pi}\oint_{\partial\Omega_b}\left(x\frac{\partial\psi_k}{\partial x} + (y-y_b)\frac{\partial\psi_k}{\partial y}\right)\mathrm{d}x, \tag{3.22b}$$

($k = 1, 2$). The force balance (2.12) and constraint (3.21) provide two algebraic equations for q and U_b. As in §3.1, the resulting equation of motion may be expressed in the form

$$\frac{U_b^{2/3}}{(1-U_b)F(W,y_b) + U_b} = \delta, \tag{3.23}$$

where now $F(W,y_b) = J_2 I_1/I_2 - J_1$. For given values of W and y_b, the value of $F(W,y_b)$ can be computed once-and-for-all, following the procedure described above, and the dependence of U_b on δ is then determined by (3.23). An analogous approach is used to compute the numerical solutions with multiple bubbles below.

We start by considering a bubble travelling along the centre-line of the channel, with $y_b = 0$, in which case it is easy to see that q must also equal zero. Hence $F(W,0) = -J_1$, and the one remaining integral can in principle be calculated using a Schwarz–Christoffel mapping (Anselmo *et al.* 2018) or approximation schemes described by Crowdy (2016); Love (1938), for example.

In figure 5(a) we examine the effects of varying the channel width W and Bretherton parameter δ. We observe that U_b is an increasing function of δ and as $\delta \to \infty$ it tends to a value strictly less than the Taylor–Saffman value $U_b = 2$. Again $\delta = 1$ is the critical value where the bubble moves with the external flow independently of the channel width, corresponding to the exact solution of the problem where $p = -x$. As in §3.1, the bubble may be accelerated or retarded by the presence of walls, depending on whether $\delta < 1$ or $\delta > 1$, respectively. In the limit of large W, the solution approaches that for an isolated bubble, as expected, while the solutions all converge to $U_b = 1$ as $W \to 2$. This latter limit corresponds to the case when the bubble exactly fits the channel width and, by conservation of mass, must travel at the same speed as the outer flow.

In figure 5(b) we study the effects of the bubble being off-centre in the channel by fixing $W = 4$ and varying y_b. Again we observe that proximity to a wall may either increase or decrease the bubble velocity, depending on whether $\delta < 1$ or $\delta > 1$, respectively, with $\delta = 1$ the critical case where $U_b = 1$ for all y_b. As in §3.1, this behaviour is caused by the liquid flowing through the gaps between the bubble and the channel walls, which either

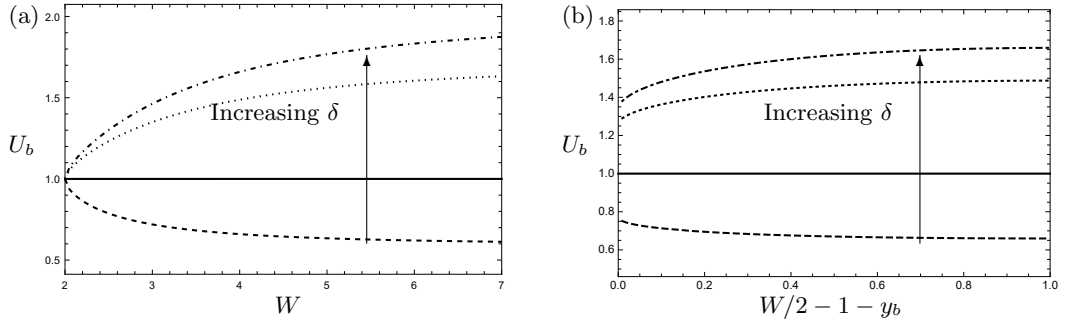

Figure 5: Bubble velocity U_b versus: (a) channel width W, with offset $y_b = 0$; (b) distance $W/2-1-y_b$ from the top channel wall, with width $W = 4$ and offset $y_b \in [0, 1]$; Bretherton parameter $\delta = 1/2$ (dashed), 1 (solid), $\delta = 5$ (dotted), $\delta = \infty$ (dot-dashed).

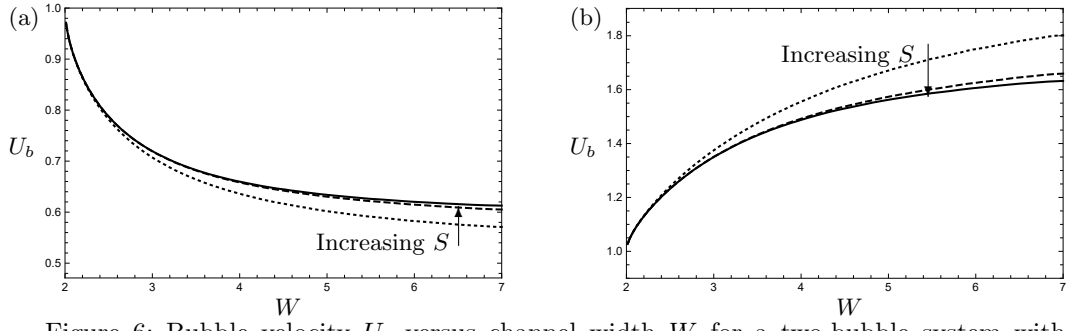

Figure 6: Bubble velocity U_b versus channel width W for a two-bubble system with separation $S = 0.2$ (dotted), 2 (dashed), single-bubble solution (solid), and (a) $\delta = 1/2$; (b) $\delta = 5$.

speeds up or slows down, thereby increasing or decreasing the average velocity at the bubble surface in equation (3.17).

3.3. *Two identical bubbles in a channel*

Next we examine a system of two identical bubbles travelling along the centre-line of the channel. Without loss of generality we take the centres of the two bubbles to be initially at $\pm(1 + S/2, 0)$, where S is the bubble separation. By symmetry, one can then show that the bubbles must both move along the centre-line with identical velocities $\boldsymbol{U}_1 = \boldsymbol{U}_2 = (U_b, 0)$.

In figure 6 we show that the two-bubble solution rapidly converges to the corresponding one-bubble solution as we increase the separation between the two bubbles, with the solutions matching up very closely even for $S = 2$. For $\delta < 1$ the bubble pair moves more slowly than a single bubble, but for $\delta > 1$ it moves more quickly. In other words, the acceleration or retardation of the liquid as it squeezes through the gaps between each bubble and the channel walls (as described in §§3.1–3.2) is suppressed by the presence of the other bubble.

3.4. *A Hele-Shaw Newton's cradle*

With three identical bubbles moving along the centre-line of a channel, we find that the bubbles in general have different speeds so, for the first time, we have to solve an unsteady problem. At each time-step we compute the three instantaneous bubble speeds

by following a similar approach to that described in §3.2, and then update the bubble positions. We again see different behaviour depending on whether $\delta < 1$ or $\delta > 1$.

At the special value $\delta = 1$, all of the bubbles move with the background flow, so the distances between them remain fixed. When $\delta < 1$, the bubbles move more slowly than the surrounding liquid. In this case we recall from §3.3 that the bubbles' speed is increased by confinement from the channel walls but decreased by the presence of a second bubble. When there are three bubbles, we find that the outer two bubbles shield the middle one from the accelerating influence of the walls. We therefore observe that the centre bubble moves backwards relative to the outer two and thus eventually becomes a pair with the rear bubble (see figure 7(a)). This qualitative behaviour has been observed experimentally by Shen *et al.* (2014); however there were surfactants in their system so a quantitative comparison with our model is not possible. The opposite effect occurs when $\delta > 1$, where now the central bubble moves faster than the outer ones and so eventually joins with the front most bubble (see figure 7(b)).

Figure 8 depicts the dependence on δ of the time T taken for the middle bubble either to be caught by the rear bubble or to catch the front bubble. The initial bubble separations are set to 1 and 0.04, as shown in figure 7(a) for $\delta < 1$ and figure 7(b) for $\delta > 1$, and we show the results for two channel widths $W = 4$ and $W = 20$. We see an asymptote at $\delta = 1$, as expected when all the bubbles travel at the same the outer fluid speed. There is also an asymptote as $\delta \to 0$, since the bubble velocities all tend to zero in this limit. As $\delta \to \infty$, T approaches a finite non-zero value that depends on W. Furthermore, we observe that T increases as we decrease the channel width, with $T \to \infty$ as $W \to 2$ for all values of δ, again because the bubbles all move at the same speed in this limit, by conservation of mass. Even at $W = 4$, the transit time is quite large for all values of δ, indicating that the difference in speed between the bubbles is relatively small.

When there are more than three bubbles, this effect can occur multiple times, as illustrated in figure 9(a) for a case with $\delta < 1$. Initially the second bubble breaks away from the front one to form a pair with the third bubble, before that pair itself breaks up so the third and fourth bubbles can form a pair. For $\delta < 1$, we recall from §3.3 that a pair of bubbles moves more slowly than an isolated bubble, so for longer times the trailing pair in figure 9(a) is left behind by the front two. Beatus *et al.* (2012) observed qualitatively similar longitudinal waves propagating backwards relative to the outer fluid flow in a series of bubbles on the centre-line of a Hele-Shaw channel, behaviour which they termed the peloton effect. However we find that the wave propagation can occur in either direction, depending on whether $\delta < 1$ or $\delta > 1$. Figure 9(b) shows a typical case with $\delta > 1$, where the initial condition is the reverse of that in figure 9(a), and the observed evolutions are almost mirror images of each other. When $\delta > 1$, a pair of bubbles travels faster than an isolated bubble, so eventually the front pair breaks away and leaves behind the other two bubbles.

The formation and breakup of successive bubble pairs observed in figure 9 is highly reminiscent of a Newton's cradle, even though there is no inertia in our system, and the motion arises solely due to viscous hydrodynamic interactions.

4. Conclusions

In this paper we develop a model for the motion of bubbles in a Hele-Shaw cell in the distinguished limit where the typical bubble aspect ratio ϵ and capillary number Ca satisfy $\mathrm{Ca}^{1/3} = O(\epsilon) \ll 1$. In this régime, each bubble remains approximately circular, and its velocity is determined by a net force balance. For an isolated bubble in an infinite Hele-Shaw cell, the model may be solved analytically, and the qualitative behaviour

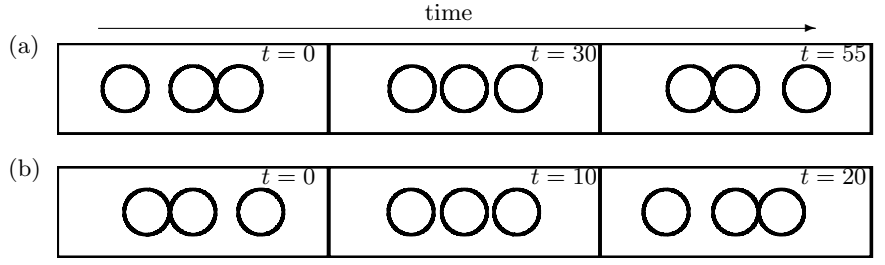

Figure 7: The progression of a series of three identical bubbles with: (a) $\delta = 1/2$; (b) $\delta = 5$.

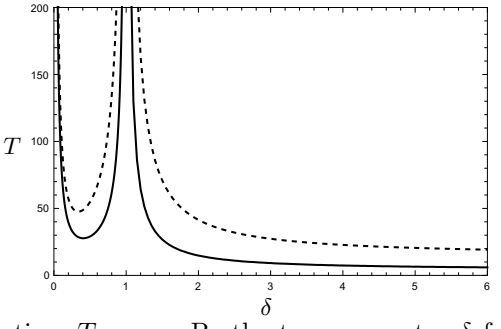

Figure 8: The transit time T versus Bretherton parameter δ for the system shown in figure 7(a) for $\delta < 1$ and figure 7(b) for $\delta > 1$, in a channel of width $W = 20$ (solid) and $W = 4$ (dashed). When $\delta < 1$ the computation starts with separations of 1 and 0.04 between the rear two and front two bubbles, respectively, and finishes when the separation between the rear two bubbles is 0.04; and *vice versa* when $\delta > 1$.

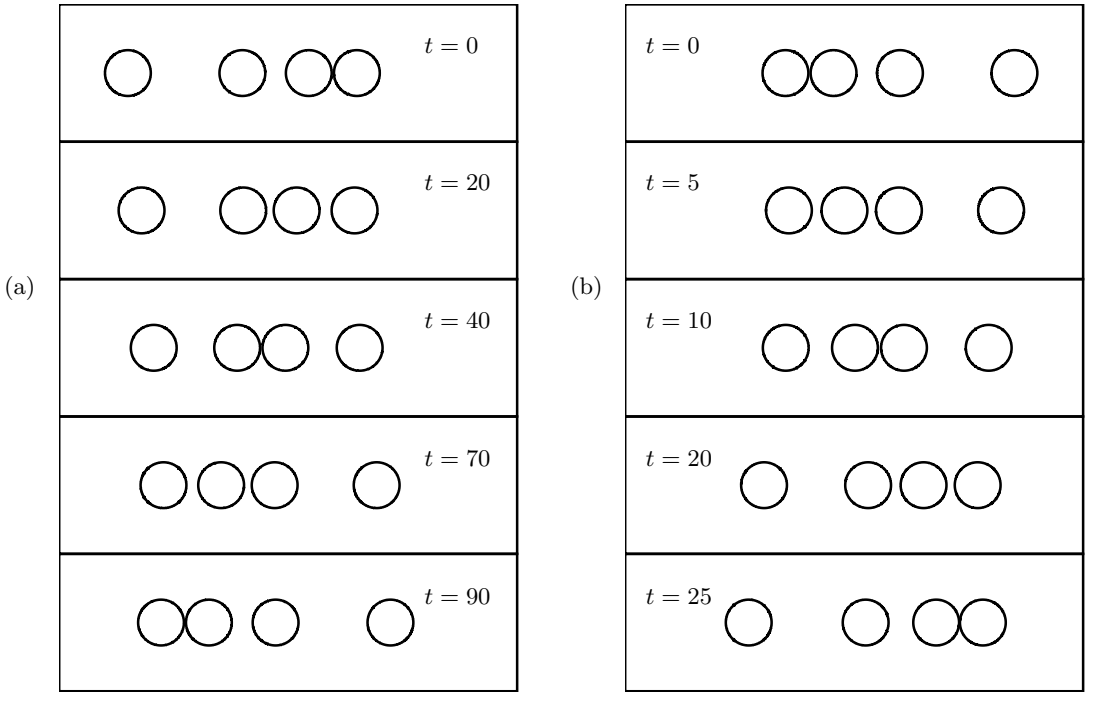

Figure 9: The progression of a series of four identical bubbles with: (a) $\delta = 1/2$; (b) $\delta = 5$.

depends on a dimensionless "Bretherton parameter", $\delta \propto \mathrm{Ca}^{1/3}/\epsilon$. In particular, the bubble moves faster than the outer fluid speed when $\delta > 1$, slower when $\delta < 1$ and precisely with the background flow if $\delta = 1$.

As shown in figure 2, the theoretically predicted bubble velocity agrees quite well with the experimental literature, but we note that very little experimental data exists for the case $\delta < 1$. The régime with $\delta < 1$ corresponds to $\mathrm{Ca} \lesssim 0.7\epsilon^3$ and, with small values of the aspect ratio ϵ (as assumed in the Hele-Shaw theory), requires extremely small values of Ca. At such very low capillary numbers, the thin films between each bubble and the cell walls become so thin that other physical effects not included in the model (e.g. disjoining pressure) may become important, leading for example to film rupture. We believe it is for this reason that the experiments at small values of δ usually include surfactants to stabilise the thin films. Our model does not at present capture the influence of surfactants on the bubble dynamics, though we note that some previous authors (e.g. Maruvada & Park 1996; Reichert *et al.* 2019) have tried to incorporate such effects in an *ad hoc* way.

When the effects of cell boundaries and multiple bubbles are included, we still observe striking changes in the qualitative behaviour depending on whether δ is greater or less than 1. For example, in a train of three identical bubbles travelling along a Hele-Shaw channel, we find that the middle bubble either catches up with the one in front (if $\delta > 1$) or is caught by the one behind (if $\delta < 1$). In longer bubble trains, we observe bubble pairs successively forming and breaking up from the front to the back of the train if $\delta < 1$ or *vice versa* if $\delta > 1$, resembling experimental observations by Beatus *et al.* (2012), for example. Although this behaviour is reminiscent of a Newton's cradle, it arises from long-range hydrodynamic interactions rather than through momentum transfer between the bubbles.

This phenomenon suggests that it is very difficult to maintain a finite stream of equally spaced identical bubbles moving along the centre-line of a Hele-Shaw channel. The bubbles are always expected to bunch up into pairs or larger aggregates, unless we are in the special case where $\delta = 1$. We do find, though, that the relative bubble velocities are often quite small, so the clustering occurs quite slowly, and it may be minimised in experiments by reducing the channel width and by keeping δ as close to 1 as possible (see figure 8). In future work we will analyse the possible instability of bubble trains to lateral perturbations, as is also often seen in experiments (Beatus *et al.* 2006; Shen *et al.* 2014).

It can be shown that the equation of motion (2.18) allows bubbles to approach and touch cell boundaries or each other in finite time. In principle our model breaks down when the distance between two bubbles (or between a bubble and a wall) becomes comparable with the cell thickness. However, it is often observed in experiments that bubbles can remain apparently stuck together without coalescing (Battat *et al.* 2022), and our model can easily be adapted to describe propagating pairs of bubbles that either remain attached or drift apart, depending on the sign of the mutual force between them.

We limit our attention in this paper to examples with relatively low numbers of equally sized and collinear bubbles. For a general system of N bubbles, our solution method would involve the numerical solution of $3N$ Dirichlet problems and computation of $9N^2$ force integrals to evaluate all of the bubble velocities at each time-step. For large N, this approach can become very slow even when the unsteady phenomena described below are neglected. An attractive alternative approach is to assume that the bubbles are sufficiently well-spaced to be approximated by dipoles, as in Beatus *et al.* (2012); Shen *et al.* (2014). In principle, dipole methods are valid only when the bubbles are well-separated; for two identical bubbles in an infinite Hele-Shaw cell, Green (2018) found that the dipole approximation works well when the bubble separation is greater than

about two bubble radii. It is the subject of current work to determine whether the dynamics we observe (e.g., in figures 7 and 9) can be adequately captured by a dipole model, even when the bubbles become arbitrarily close and the dipole approach is not strictly valid.

Figure 2 shows that the speed of an isolated bubble is an increasing function of its radius. In examples with many non-identical bubbles, the dynamics depends on the relative sizes of neighbouring bubbles, as well as on the bubble interaction effects seen in figures 7 and 9, for example. In microfluidic experiments and devices, the bubble radii are often almost but not precisely uniform, and the resulting delicate balance between size effects and interaction effects is also the subject of current research.

As promised in §2, we now discuss the validity of the boundary condition (2.3*b*). At the front interface of a moving bubble, the additional pressure drop (proportional to $\mathrm{Ca}_n^{2/3}$) may be derived by solving Bretherton's problem for a meniscus advancing with effective capillary number Ca_n (Bretherton 1961). As noted by Reichert *et al.* (2019), this approach is invalid close to points where Ca_n changes sign. Burgess & Foster (1990) showed that the discontinuous term in (2.3*b*), involving the function β, is smoothed out in "lateral transition regions" (LTRs) where $\mathrm{Ca}_n = O(\epsilon^{3/5}\mathrm{Ca}^{1/5})$. In the distinguished limit studied here, Ca is assumed to be of order ϵ^3, and it follows that *the LTRs contribute corrections of order* $\epsilon^{6/5}$ *to the force balance* (2.10). Since other corrections of order ϵ have already been neglected, we conclude that these effects are indeed negligible in our model.

At a retreating meniscus, as well as the local value of Ca_n, the additional pressure drop depends also on the thickness of the liquid films between the bubble and the cell walls into which the interface is propagating. In general, this dependence leads to a drag coefficient of the form

$$\beta(\mathrm{Ca}_n) = \mathcal{F}\left(\mathrm{Ca}_n^+/\mathrm{Ca}_n\right) \tag{4.1}$$

when $\mathrm{Ca}_n < 0$, where Ca_n^+ is the normal capillary number at the corresponding point on the front interface which deposited the thin films currently being consumed by the rear interface, and the function $\mathcal{F}$ has been calculated e.g. by Burgess & Foster (1990). For a circular bubble moving at constant velocity, we have $\mathrm{Ca}_n^+ \equiv \mathrm{Ca}_n$, so $\beta(\mathrm{Ca}_n) = \mathcal{F}(1) = \beta_2$ whenever $\mathrm{Ca}_n < 0$, as in (2.4). For a non-circular bubble moving at constant velocity, the argument of the function $\mathcal{F}$ in (4.1) is equal to $\mathrm{Ca}_n^+/\mathrm{Ca}_n = \cos\theta_+/\cos\theta_-$, where $\theta_\pm$ are the angles made with the direction of motion at corresponding points on the front and rear bubble interfaces (Burgess & Foster 1990).

The situation is more complicated when the motion is unsteady, even if the bubbles remain (approximately) circular, as assumed in this paper. According to (4.1), the pressure drop across the rear meniscus depends on the normal velocity at the front meniscus at some previous time, and the force balance (2.18) thus produces an integral equation rather than an algebraic equation for the bubble velocity. As a first approximation, we can justify ignoring such effects in the unsteady multi-bubble solutions shown in §3.4 by observing that the computed bubble velocities are slowly varying (on a typical transit time-scale $\hat{R}/\hat{U}$). Nevertheless, it is the subject of current research to quantify the impact of non-local dynamics on the bubble motion in general.

Acknowledgements

The authors are grateful for conversations with Howard Stone, Janine Nunes and Katie Wu. IMG is grateful to the Royal Society for funding through a University Research Fellowship. DJB is grateful to EPSRC, grant reference number EP/V520202/1, for funding.

Declaration of interests

The authors report no conflict of interest.

REFERENCES

Anna, S. L. 2016 Droplets and bubbles in microfluidic devices. *Ann. Rev. Fluid Mech.* **48**, 285–309.

Anselmo, T., Nelson, R., Carneiro da Cunha, B. & Crowdy, D. G. 2018 Accessory parameters in conformal mapping: exploiting the isomonodromic tau function for Painlevé VI. *Proc. R. Soc. London, Ser. A* **474** (2216), 20180080.

Askey, R. 1978 The q-gamma and q-beta functions. *Appl. Anal.* **8** (2), 125–141.

Battat, S., Weitz, D. A. & Whitesides, G. M. 2022 Nonlinear phenomena in microfluidics. *Chem. Rev.* **122** (7), 6921–6937.

Beatus, T., Bar-Ziv, R. H. & Tlusty, T. 2012 The physics of 2D microfluidic droplet ensembles. *Phys. Rep.* **516** (3), 103–145.

Beatus, T., Tlusty, T. & Bar-Ziv, R. 2006 Phonons in a one-dimensional microfluidic crystal. *Nat. Phys.* **2** (11), 743–748.

Bretherton, F. 1961 The motion of long bubbles in tubes. *J. Fluid Mech.* **10** (2), 166–188.

Burgess, D. & Foster, M. R. 1990 Analysis of the boundary conditions for a Hele-Shaw bubble. *Phys. Fluids A* **2** (7), 1105–1117.

Crowdy, D. 2008 Explicit solution for the potential flow due to an assembly of stirrers in an inviscid fluid. *J. Eng. Math.* **62** (4), 333–344.

Crowdy, D. 2009 Multiple steady bubbles in a Hele-Shaw cell. *Proc. R. Soc. London, Ser. A* **465** (2102), 421–435.

Crowdy, D. G. 2016 Uniform flow past a periodic array of cylinders. *Eur. J. Mech. B. Fluids* **56**, 120–129.

Garstecki, Piotr, Gitlin, Irina, DiLuzio, Willow, Whitesides, George M, Kumacheva, Eugenia & Stone, Howard A 2004 Formation of monodisperse bubbles in a microfluidic flow-focusing device. *Applied Physics Letters* **85** (13), 2649–2651.

Gnyawali, V., Moon, B.U., Kieda, J., Karshafian, R., Kolios, M. C. & Tsai, S. S. H. 2017 Honey, I shrunk the bubbles: microfluidic vacuum shrinkage of lipid-stabilized microbubbles. *Soft Matter* **13** (22), 4011–4016.

Green, Y. 2018 Approximate solutions to droplet dynamics in Hele-Shaw flows. *J. Fluid Mech.* **853**, 253–270.

Halpern, D. & Jensen, O. E. 2002 A semi-infinite bubble advancing into a planar tapered channel. *Phys. Fluids* **14** (2), 431–442.

Huerre, A., Miralles, V. & Jullien, M.-C. 2014 Bubbles and foams in microfluidics. *Soft Matter* **10** (36), 6888–6902.

Kopf-Sill, A. R. & Homsy, G. M. 1988 Bubble motion in a Hele-Shaw cell. *Phys. Fluids* **31** (1), 18–26.

Kreyszig, E. 1959 *Differential Geometry*. University of Toronto Press.

Love, A. E. H. 1938 Electrostatic problems related to a perforated strip. *Q. J. Math.* **os-9** (1), 246–258.

Maruvada, S. R. K. & Park, C.-W. 1996 Retarded motion of bubbles in Hele-Shaw cells. *Phys. Fluids* **8** (12), 3229–3233.

Meiburg, E. 1989 Bubbles in a Hele-Shaw cell: Numerical simulation of three-dimensional effects. *Phys. Fluids A* **1** (6), 938–946.

Park, C.-W. & Homsy, G. M. 1984 Two-phase displacement in Hele-Shaw cells: theory. *J. Fluid Mech.* **139**, 291–308.

Park, C.-W., Maruvada, S. R. K. & Yoon, D.-Y. 1994 The influence of surfactant on the bubble motion in Hele-Shaw cells. *Phys. Fluids* **6** (10), 3267–3275.

Reichert, B., Cantat, I. & Jullien, M.-C. 2019 Predicting droplet velocity in a Hele-Shaw cell. *Phys. Rev. Fluids* **4** (11), 113602.

Reinelt, D. A. 1987 Interface conditions for two-phase displacement in Hele-Shaw cells. *J. Fluid Mech.* **183**, 219–234.

Reyssat, E. 2014 Drops and bubbles in wedges. *J. Fluid Mech.* **748**, 641–662.

Salem, A. 2012 A completely monotonic function involving q-gamma and q-digamma functions. *J. Approximation Theory* **164** (7), 971–980.

Sarig, I., Starosvetsky, Y. & Gat, A. D. 2016 Interaction forces between microfluidic droplets in a Hele-Shaw cell. *J. Fluid Mech.* **800**, 264–277.

Shen, B., Leman, M., Reyssat, M. & Tabeling, P. 2014 Dynamics of a small number of droplets in microfluidic Hele-Shaw cells. *Exp. Fluids* **55** (5), 1–10.

Tanveer, S. 1986 The effect of surface tension on the shape of a Hele-Shaw cell bubble. *Phys. Fluids* **29** (11), 3537–3548.

Taylor, G. & Saffman, P. G. 1959 A note on the motion of bubbles in a Hele-Shaw cell and porous medium. *Q. J. Mech. Appl. Math.* **12** (3), 265–279.

Tchieu, A. A., Crowdy, D. & Leonard, A. 2010 Fluid-structure interaction of two bodies in an inviscid fluid. *Phys. Fluids* **22** (10), 107101.

Vasconcelos, G. L. 1994 Multiple bubbles in a Hele-Shaw cell. *Phys. Rev. E* **50** (5), R3306.

Wong, H., Radke, C. J. & Morris, S. 1995 The motion of long bubbles in polygonal capillaries. Part 2. Drag, fluid pressure and fluid flow. *J. Fluid Mech.* **292**, 95–110.